Immunologic and Biophysical Features of the BNT162b2 JN.1- and KP.2-Adapted COVID-19 Vaccines

Authors

Wei Chen[1*], Kristin R. Tompkins[1*], Ian W. Windsor[2*], Lyndsey T. Martinez[1], Minah Ramos[1], Weiqiang Li[1], Shikha Shrivastava[1], Swati Rajput[1], Jeanne S. Chang[2], Parag Sahasrabudhe[2], Kimberly F. Fennell[2], Thomas J. McLellan[2], Graham M. West[2], Kristianne P. Dizon[1], Aaron Yam[1], Siddartha Mitra[1], Subrata Saha[1], Daiana Sharaf[1], Andrew P. McKeen[3], Carla I. Cadima[4], Alexander Muik[4], Wesley Swanson[1], Raquel Munoz Moreno[1], Pilar Mendoza Daroca[1], Ugur Sahin[4], Annaliesa S. Anderson[1], Huixian Wu[2], Kena A. Swanson[1‡] & Kayvon Modjarrad[1‡]

* Contributed equally

‡ Corresponding authors: kayvon.modjarrad@pfizer.com, kena.swanson@pfizer.com

Affiliations

[1]Pfizer Vaccine Research and Development; Pearl River, NY, USA.

[2]Pfizer Discovery Sciences; Groton, CT, USA.

[3]Pfizer Global Biometrics and Data Management; Pearl River, NY, USA.

[4]BioNTech; Mainz, Germany.

ABSTRACT Vaccines remain a vital public health tool to reduce the burden of COVID-19. COVID-19 vaccines that are more closely matched to circulating SARS-CoV-2 lineages elicit more potent and relevant immune responses that translate to improved real-world vaccine effectiveness. The rise in prevalence of the Omicron JN.1 lineage, and subsequent derivative sublineages such as KP.2 and KP.3, coincided with reduced neutralizing activity and effectiveness of Omicron XBB.1.5-adapted vaccines. Here, we characterized the biophysical and immunologic attributes of BNT162b2 JN.1- and KP.2-adapted mRNA vaccine-encoded spike (S) protein immunogens. Biophysical interrogations of S revealed the structural consequences of hallmark amino acid substitutions and a potential molecular mechanism of immune escape employed by JN.1 and KP.2. The vaccine candidates were evaluated for their immunogenicity when administered as fourth or fifth doses in BNT162b2-experienced mice or as a primary series in naïve mice. In both vaccine-experienced and naïve settings, JN.1- and KP.2-adapted vaccines conferred improved neutralizing responses over the BNT162b2 XBB.1.5 vaccine against a broad panel of emerging JN.1 sublineages, including the predominant KP.3.1.1 and emerging XEC lineages. Antigenic mapping of neutralizing responses indicated greater antigenic overlap of JN.1- and KP.2-adapted vaccine responses with currently circulating sublineages compared to an XBB.1.5-adapted vaccine. $CD4^+$ and $CD8^+$ T cell responses were generally conserved across all three vaccines. Together, the data support the selection of JN.1- or KP.2-adapted vaccines for the 2024-25 COVID-19 vaccine formula.

KEYWORDS

COVID-19; SARS-CoV-2; BNT162b2; mRNA vaccine; preclinical; variants; immunogenicity; spike protein; structure; cryogenic-electron microscopy

ONE-SENTENCE SUMMARY

The Omicron JN.1- and KP.2-adapted BNT162b2 mRNA vaccines encoding prefusion S proteins elicit similar preclinical neutralizing antibody responses against circulating JN.1 sublineage pseudoviruses that are more potent than those elicited by past iterations of BNT162b2 licensed vaccines, thus demonstrating the importance of annual strain changes to the COVID-19 vaccine.

INTRODUCTION

As coronavirus disease-2019 (COVID-19) transitions from a pandemic to an endemic state, questions remain around the evolutionary trajectory of its causative pathogen, Severe Acute Respiratory Syndrome Coronavirus-2 (SARS-CoV-2), the periodicity of its incidence, and the necessary frequency of variant-adapted vaccine updates to ensure optimal protection against a range of clinical outcomes. It remains clear, however, that the annual burden of COVID-19 cases, hospitalizations and deaths still places it among the leading global causes of infectious disease morbidity and mortality, similar to or higher than pre-pandemic levels observed for influenza and other pneumonias [1-4].

Since the emergence of the first SARS-CoV-2 Omicron variant of concern (VOC) in late 2021, the virus has differentiated into more than 4300 distinct genetic lineages [5]. As these lineages have trended toward increased transmissibility and greater antigenic distance from the original ancestral strain, approved vaccines have been updated to include variant-specific mutations in the SARS-CoV-2 spike (S) [6-10], to maintain optimal protection against the most relevant lineages causing COVID-19. Although updated vaccines have been typically introduced to the general public during the early Autumn season of the Northern Hemisphere, vaccine manufacturers must conduct at-risk development activities throughout the preceding year in anticipation of the variant

69 composition recommendations issued by regulators and international normative bodies in the
70 Spring of that year [9-11].

71 During the Northern Hemisphere Winter of 2023 to 2024, the variant epidemiology of
72 SARS-CoV-2 shifted from a dominance of Omicron XBB derivative lineages to BA.2.86
73 descendants, most notably the variant of interest, JN.1 [12] and its sublineages, achieving a peak
74 prevalence that exceeded all prior Omicron lineages since the emergence of BA.1 and BA.2. As
75 the global dominance of JN.1 plateaued and declined in prevalence, derivative sublineages
76 acquired additional mutations, translating to amino acid substitutions in the S protein that
77 conferred improved viral fitness or immune escape. Some of those sublineages (*e.g.*, KP.2) gained
78 epidemiologic relevance during the summer months of 2024, particularly those that contained
79 convergent F456L and R346T amino acid substitutions in the S receptor binding domain (RBD).
80 More recently, the KP.3 sublineage, which contains the F456L, but not the R346T substitution,
81 has emerged as globally dominant, likely owing to its acquisition of the Q493E substitution, also
82 located within the RBD. This sublineage and its derivatives, particularly KP.3.1.1, now account
83 for most SARS-CoV-2 infections [13].

84 The JN.1 cluster of sublineages occupies a unique antigenic space separate from all other
85 prior Omicron lineages. Real-world studies of the XBB.1.5-adapted COVID-19 vaccines
86 demonstrated robust immune response and effectiveness against XBB lineages that diminished
87 in response to the BA.2.86 and JN.1 lineages [14-19]. To better understand the structural and
88 functional consequences of the antigenic shift from this new lineage cluster, and subsequent
89 antigenic drift within it, we evaluated the biophysical and immunologic features of the prefusion-
90 stabilized full-length SARS-CoV-2 S-proteins of JN.1 and KP.2. To our knowledge, we present
91 the first in-depth structural analysis of JN.1 and KP.2 full-length, prefusion-stabilized S

immunogens, building prior reports detailing the impact of JN.1 sublineage-specific S mutations on neutralization resistance. We also assessed whether an Omicron JN.1 or KP.2-updated BNT162b2 vaccine could improve immune responses that are important for conferring protection against COVID-19 [20], against the JN.1 lineage and a panel of contemporary JN.1-derived sublineages, as compared to the BNT162b2 XBB.1.5 vaccine.

Both monovalent JN.1- and KP.2-adapted COVID-19 vaccines have been recommended for the 2024-2025 formula. The two lineages differ in their S amino acid sequences by 3 residues [21]. In prior years, small genetic differences have not necessarily translated into antigenic differences. Given that two variant-adapted vaccines have been introduced in the same season, we sought to understand the impact of these few, but potentially consequential, genetic differences on biophysical, structural and immunologic attributes of vaccine-encoded JN.1 and KP.2 prefusion stabilized S proteins. The BNT162b2 JN.1 and KP.2 vaccines use the same mRNA backbone as prior approved versions of BNT162b2 and are minimally modified to contain lineage-specific sequence changes of the SARS-CoV-2 prefusion stabilized S protein that has been evaluated in previous preclinical and clinical studies . We employed a vaccine-experienced murine model, with varying schedules of prior vaccination regimens, together with a vaccine-naïve murine model, to assess humoral and cellular immunogenicity, so as to approximate the diversity of the immune-experience of the general population across all age groups [22]. An evaluation of both structural and functional consequences of the most recent evolution of SARS-CoV-2 lineages in varied models may then elucidate the potential impact on vaccine performance.

METHODS

115 **SARS-CoV-2 S(P2) and RBD Protein Expression and Purification**

116 Protein sequences of the full-length prefusion stabilized S(P2) of the SARS-CoV-2 JN.1 lineage
117 and KP.2 sublineage contained amino acid changes relative to the ancestral Wuhan-Hu-1 S
118 (GenBank accession number: MN908947.3) as listed in Table S1**Error! Reference source not**
119 **found.**. S(P2) contains two proline substitutions at residues 986 and 987 (K986P, V987P) and
120 utilizes a C-terminal TwinStrep tag. The RBD constructs contain an N-terminal S protein leader
121 peptide and coding regions from 321-527 for JN.1 and KP.2, and 327-528 for the ancestral strain,
122 followed by a C-terminal affinity tag as indicated in Table S1. Details on S(P2) and RBD protein
123 expression and purification can be found in the Supplementary Materials.

124

125 **Stability of Wild Type (WT), Omicron JN.1 and KP.2 FL S(P2) by Thermal Shift Assay**
126 **(TSA)**

127 Stability of FL S(P2) proteins was measured by Tycho NT.6 (NanoTemper, firmware version:
128 1.10.3) as described previously [23]. The inflection temperature for each thermal melting curve
129 reported by the Tycho NT.6 software was reported as the thermal melting temperature (T_m) of
130 S(P2) proteins.

131

132 **Binding Kinetics of Purified FL S(P2) Protein and RBD to Immobilized Human ACE-2-PD**

133 FL S(P2) and RBD proteins of JN.1, KP.2 and WT strains were assessed by biolayer
134 interferometry (BLI) binding to immobilized human ACE-2-PD, as described previously [23].

135

136 **Cryogenic Electron Microscopy (Cryo-EM) of JN.1 and KP.2 S(P2)**

137 SARS-CoV-2 FL S(P2) (K986P and V987P substituted) proteins of the JN.1 and KP.2 lineages
138 were interrogated by electronic cryogenic electron microscopy (cryo-EM) analysis following
139 membrane extraction and purification. Grids were prepared with JN.1 and KP.2 S(P2) proteins at
140 5.6 and 5.8 mg/ml by applying 4 µL to Quantifoil R1.2/1.3 200 mesh gold grids that were glow-
141 discharged for 60 seconds at 15 mA in a Pelco easiGlow cleaning system and blotted for 3 seconds
142 with a blot force of +3 before plunging into liquid nitrogen-cooled liquid ethane using a Mark IV
143 Vitrobot with a sample chamber maintained at 4°C and 100% humidity. Data collection was
144 performed with a Titan Krios G2 electron microscope operated at 300 kV, controlled by EPU,
145 and equipped with a Falcon 4i direct electron detector and Selectris energy filter configured with
146 a 10 eV slit (ThermoFisher Scientific). A total of 7k and 9k movies were collected for JN.1 and
147 KP.2 S(P2) protein samples with a total dose of 40.0 $e^-/Å^2$ and a -0.4 µm to -2.4 µm defocus range.
148 Details on cryo-EM data processing and model building can be found in the Supplementary
149 Materials and Table S3.
150
151 **Mass Spectrometry Characterization of JN.1 and KP.2 S(P2) N-linked Glycosylation**
152 Mapping of N-linked glycosylation sites was conducted on recombinant purified JN.1 and KP.2
153 S(P2) as described previously [23]. For glycosylation complexity determination, S(P2) protein
154 digests, before and after O18 water and PNGase F treatment, were analyzed using liquid
155 chromatography-mass spectrometry (LC-MS). The data were processed using Protein Metrics
156 PMI-Byos Byologic PTM workflow with glycan modifications enabled. Relative levels of the
157 various glycan forms were determined by summing the extracted ion chromatogram peak areas
158 for all detected charge states and forms for a given isobaric glycosylation state. Relative

159 estimation of abundance was obtained by comparing frequencies of different glycans, with an
160 assumption that all glycopeptides have similar ionization.
161
162 **Animal Ethics**
163 All mouse studies were performed at Pfizer, Inc. (Pearl River, NY, USA), an Association for
164 Assessment and Accreditation of Laboratory Animal Care (AAALAC) accredited facility.
165 Animals were observed after all procedures and injection sites were monitored following each
166 vaccination. All procedures performed on animals were in accordance with regulations and
167 established guidelines and were reviewed and approved by an Institutional Animal Care and
168 Use Committee or through an ethical review process.
169
170 **Immunogenicity Studies**
171 *4th or 5th Vaccination in BNT162b2-Experienced Mice*
172 Monovalent XBB.1.5, JN.1, and KP.2-adapted BNT162b2 vaccines were evaluated as either a
173 4th or 5th dose in female BALB/c mice (10 per group; Jackson Laboratory). In the 5th dose study,
174 mice were vaccinated intramuscularly (i.m.) at 6-8 weeks of age with 2-doses (Day 0, 21) of
175 original BNT162b2 WT vaccine, followed by a 3rd dose booster (Day 49) of bivalent WT +
176 Omicron BA.4/5 vaccine, a 4th dose (Day 84) of the monovalent Omicron XBB.1.5 adapted
177 vaccine, and a 5th dose (Day 111) of either the monovalent XBB.1.5, JN.1, or KP.2-adapted
178 vaccine. All vaccinations used a 0.5 µg total dose in a 50 µL volume (bivalent formulations
179 contained equal quantities of each mRNA, 0.25 µg each). A control group of five mice received
180 saline injections (50 µL) according to the same schedule, in place of active vaccines. Sera were
181 collected for evaluation of pseudovirus neutralizing antibody responses prior to the 5th dose

182 (Day 111) and at the study end (Day 140). Spleens were collected from all mice at Day 140 to
183 evaluate cell-mediated immune responses (Fig. S4A).
184 In the 4th dose study, female BALB/c mice (10 per group; Jackson Laboratory) were first
185 vaccinated i.m. at 6-8 weeks of age and subsequent doses were administered according to the
186 same schedule as the 5th dose study, except that the 4th dose was administered on Day 64 as
187 either the monovalent XBB.1.5, JN.1, or KP.2-adapted vaccine and there was no 5th dose. As
188 above, sera were collected for evaluation of pseudovirus neutralization responses prior to the 4th
189 dose (Day 64) and two weeks later at study end (Day 78) (Fig. S4B).
190
191 *2-Dose Primary Series in Naïve Mice*
192 Female BALB/c mice (10 per group Jackson Laboratory) were vaccinated i.m. at 6-8 weeks of
193 age on Days 0 and 21 with either monovalent XBB.1.5, JN.1, or KP.2-adapted vaccine. As
194 described above, vaccine formulations contained a total dose level of 0.5 µg mRNA in a 50 µL
195 volume and a control group (10 mice) received saline injections adjacent to the vaccine groups.
196 Sera and spleens (5 mice/group) were collected 28 days after the second dose (day 49) for
197 evaluation of pseudovirus neutralizing antibody responses and cell-mediated immune responses,
198 respectively (Fig. S4C).
199
200 **VSV-SARS-CoV-2 S Pseudovirus Neutralization Assay**
201 The pseudovirus neutralization assay (PNA) was defined and performed as previously described
202 [23]. VSV-based pseudoviruses contained the S protein from the following SARS-CoV-2 lineages:
203 WT (Wuhan-Hu-1, ancestral strain), BA.4/5, XBB.1.5, JN.1, JN.1.6,1, JN.1.7, JN.1.13.1,
204 KW.1.1, KP.2, KP.2.2, KP.1.1, KS.1, JN.1.16.1, KZ.1.1.1, KP.2.3, KP.3, KP.3.1.1, LB.1 and

205 XEC. Amino acid sequence substitutions relative to JN.1 for all tested pseudoviruses are
206 provided in Fig. S5.
207
208 **Omicron XBB.1.5, JN.1 and KP.2 Antigenic Cartography**
209 Antigenic maps were constructed using the antigenic cartography toolkit Racmacs v1.2.9
210 (https://acorg.github.io/Racmacs/index.html). In brief, antigenic cartography is a method to
211 quantify and visualize neutralization data. An antigenic map takes titration data that measures
212 strength of reactivity of a group of antisera (sera where an individual mouse has been vaccinated
213 with a unique antigen of a particular SARS-CoV-2 lineage) against a group of antigens
214 (different SARS-CoV-2 lineages). Antigenic mapping uses multidimensional scaling to position
215 antigens (viruses) and sera in a map to represent their antigenic relationships. Antigenically
216 similar strains are spatially close to one another on the map, while antigenically distinct strains
217 are further apart. The spacing between grid lines is 1 unit of antigenic distance, corresponding
218 to a two-fold dilution of antiserum in the neutralization assay. The maps were constructed by
219 Racmacs package in R using 2000 optimizations, with the minimum column basis parameter set
220 to "none."
221
222 **T-cell Response by Flow Cytometry Assay**
223 Murine splenocytes were stimulated *ex vivo* as previously described (*1*) with DMSO only
224 (unstimulated) or specific amino acid (aa) peptide libraries (15aa, 11aa overlap, 1 to 2
225 µg/mL/peptide) representing SARS-CoV-2 S amino acid sequences. Five individual peptide
226 pools represented the full-length S sequence of the ancestral Wuhan (WT) (JPT), BA.4/5 (JPT),
227 XBB.1.5 (JPT), JN.1 (JPT) and KP.2 lineages (Mimotopes). Following stimulation, splenocytes

228 were stained for CD154 (CD40L), IFN-γ, TNF-α, and IL-2 positive $CD4^+$ and $CD8^+$ T cells, as
229 previously described [23]. Samples were acquired on a 5-Laser Aurora system (Cytek ®) using
230 SpectroFlo® software (version 3.1.2). The instrument was subject to daily quality control
231 procedures using SpectroFlo® QC Beads per manufacturer recommendations. Acquired data files
232 were analyzed using OMIQ® software. The T cell gating strategy is shown in Fig. S6.
233
234 **Data Availability Statement**
235 The final full-length S(P2) cryo-EM density maps and models for the JN.1 (3-down and 1-up)
236 and KP.2 (3-down, 1-up, and 2-up) conformations are deposited in the Electron Microscopy
237 Data Bank (EMDB) and the Protein Data Bank (PDB) under accession codes EMD-46637 and
238 PDB ID 9D8H, EMD-46638 and PDB ID 9D8H, EMD-46639 and PDB ID 9D8I, EMD-46640
239 and PDB ID 9D8J, and EMD-46641 and PDB ID 9D8K, respectively.
240
241 **Statistical Analysis**
242 Mouse immunogenicity data were analyzed using SAS version 9.4. All statistical analyses were
243 performed using ANOVA on log-transformed data. Comparisons were made on mouse sera
244 across pseudoviruses at the last post-vaccination timepoint of each study with Dunnett's test for
245 multiple comparisons. For intergroup comparisons, the XBB.1.5 vaccine group was the
246 reference; for intragroup comparisons (pseudoviruses within a vaccine group), the vaccine
247 target lineage (XBB.1.5, JN.1 or KP.2) served as the reference. All tests were two-tailed. A
248 p-value of less than 0.05 was considered statistically significant.
249
250 **RESULTS**

251 **Enhanced ACE2 receptor binding and reduced thermostability of JN.1 and KP.2 S proteins**
252 **compared to WT SARS-CoV-2 S protein**

253 Full-length prefusion-stabilized S(P2) proteins of Wuhan-Hu-1 (WT), Omicron JN.1, and KP.2
254 were expressed from DNA corresponding to the adapted BNT162b2 RNA coding sequences
255 using similar methods as previously reported[23]. All S(P2) proteins were expressed on the cell
256 surface following in vitro transfection of Expi293F cells and showed similar binding to human
257 ACE2 (Fig. S1A). Analysis of membrane-extracted and affinity-purified full-length S(P2)
258 showed a single peak by size exclusion chromatography (SEC), with S predominantly cleaved
259 into S1 and S2 subunits (Fig. 1A and Fig. S1B). Thermal shift assay (TSA) analyses showed the
260 melting temperature (T_m) of JN.1 (61.6 ± 0.24 ° C) and KP.2 (60.1 ± 0.19 ° C) were similar to
261 one another (Fig. 1B) and approximately 5-7 °C lower than WT S(P2) (67.1 ± 0.17 °C) [23].
262 Biolayer interferometry (BLI) analysis of purified RBDs only, which contain the receptor binding
263 motif (RBM) critical for ACE2 binding, showed significantly increased binding of soluble JN.1
264 and KP.2 RBDs to fixed human ACE2 peptidase domain (ACE2-PD) (K_D 1.70 nM and 2.07 nM,
265 respectively) compared to the WT RBD (K_D 31.3 nM) [23] (Fig. 1C).

266

267 **Acquisition of glycosylation sites within the JN.1 and KP.2 S proteins**

268 The purified S(P2) proteins of JN.1 and KP.2 were analyzed by liquid chromatography mass
269 spectrometry (LCMS) to identify N-linked glycosylation sites. Glycosylation mapping confirmed
270 that JN.1 and KP.2 have conserved glycosylation sites on the S protein, despite undergoing
271 extensive mutations compared to WT S. This is consistent with previous studies of earlier lineages,
272 suggesting a correlation between viral fitness and glycosylation [24]. Compared to XBB.1.5, we
273 discovered two new glycosylation sites (Table 1) in the RBD and N-terminal domain (NTD) of

274 JN.1 and KP.2 S, respectively. The novel RBD glycosylation site is located on N354 which is
275 gained by the K356T substitution, whereas the novel NTD glycosylation site is a result of the
276 H245N substitution within the peptide ALN[245]RSYLT. Analysis of the glycosylation
277 heterogeneity confirmed that both sites are fully modified by glycans with a major composition
278 being HexNAc(2)Hex(5) (Table S2).
279
280 **JN.1 and KP.2 S(P2) cryo-EM structure**
281 Structures of JN.1 and KP.2 full-length, prefusion stabilized SARS-CoV-2 S proteins were solved
282 by cryo-EM to validate the conformation of the encoded antigen of both vaccines and to evaluate
283 the structural consequences of the lineages' hallmark mutations in the context of S(P2). Both JN.1
284 and KP.2 S(P2) proteins exhibited prefusion conformations, as anticipated. The cryo-EM
285 processing employed herein sought to identify all RBD (up/down) configurations (Fig. S2) within
286 the S trimer. Unlike the WT S(P2) protein, which was predominantly (~80%) found in the 3-down
287 conformation[25], the prefusion-stabilized JN.1 S protein was observed in the 3-down (65%)
288 conformation, and at a lower frequency in a 1-up (35%) conformations, while KP.2 S was more
289 evenly observed in 3-down (41%) and 1-up (48%) conformations, with a small fraction in a 2-up
290 (11%) conformation, indicating KP.2 exhibits a greater tendency than earlier variants for adopting
291 the RBD-up conformations (Fig. 2A).
292 In both JN.1 and KP.2 S, the C3-symmetric, 3-down conformation of the RBD core is
293 resolved at ~4Å, whereas the receptor binding motif (RBM), comprising residues 450-490, were
294 absent at high resolution. In the 1-up conformations, the RBM was best resolved for the down-
295 RBD adjacent to the up-RBD (Fig. S3). The RBM of the down-RBD, adjacent to the up-RBD,

296 was poorly resolved, though it contained high-resolution features for the core. In contrast, very
297 little of the second up-RBD was seen in the 2-RBD-up KP.2 structure (Fig. S3).

298 Structural changes for both lineages were likely caused by two amino acid substitutions
299 shared by JN.1 and KP.2—P621S and P1143L—that differentiate them from XBB.1.5. The P621
300 residue is in a region of the S subdomain 2 (SD2) called the 630 loop that is unstructured in full-
301 length, 2P-stabilized XBB.1.5 and Wuhan S protein cryo-EM densities. Despite being situated in
302 this unstructured region, the P621S substitution leads to a well-resolved alpha helix (Fig. 2B).
303 The structured region is found in every protomer of the five solved structures of the JN.1 and
304 KP.2 S proteins. In the context of the 1-up RBD structures of JN.1 and KP.2, a region adjacent to
305 the 630 helix—residues 829-848 or the fusion peptide proximal region (FPPR) of the adjacent
306 protomer—is also well-resolved (Fig. 2B, Fig. S3). Though lower in resolution, there is a clear
307 density, including a disulfide bond between C836 and C847. As a result, the structured FPPR
308 interacts with the 630-helix from the adjacent protomer, contributing to an enhanced
309 interprotomer stability which may reduce S1/S2 shedding in the context of the RBD-up
310 conformation. The P1143 residue is located near the N-terminus of the stem helix. The cryo-EM
311 density revealed two discrete conformations of the stem for both JN.1 and KP.2 S. The alternative
312 poses were best resolved in the JN.1 3-down, C3-symmetry reconstruction (Fig. 2C, Fig. S3) and
313 diverge near the mutated proline residue.

314 Two additional mutations, H245N and K356T, differentiate JN.1 and KP.2 from XBB.1.5
315 and earlier lineages, and are shared with the parental BA.2.86 lineage. These mutations have
316 yielded novel glycosylation sites that were fully glycosylated in the resolved structures (Fig. 2D,
317 Tables 2 and S1). However, H245N within the NTD is located in a low-resolution region of the
318 EM densities of the two JN.1 and three KP.2 structures. As a result, the possible glycosylation

319 modification of H245N is absent from the cryo-EM map reconstruction. The K356T mutation led
320 to glycosylation at N354 in JN.1, KP.2 and previous variants harboring the mutation [26,27]. This
321 glycan is located near the interface of the RBD and the NTD of an adjacent protomer (Fig. 2D).
322 Overall, JN.1 and KP.2 S proteins differ by three residues: R346T and F456L in the RBD
323 and V1104L in the S2 domain. R346T has been observed in several earlier lineages and may
324 impact antibodies recognizing the RBD class 3 epitope [28]. The V1104L mutant residue exhibited
325 density consistent with the additional methylene group and no discernable structural changes.
326 F456L is located in the RBM and in a relatively low-resolution region of the map. Of note, the
327 RBD is best resolved in the down conformation adjacent to the up conformation and the mutant
328 L456 is located at the protomer interface (Fig. 2D, Fig. S3).
329

330 **BNT162b2 JN.1- and KP.2-adapted vaccines neutralizing responses to JN.1 sublineages in**
331 **a vaccine-experienced mouse model**

332 BNT162b2 JN.1- and KP.2-adapted vaccines were evaluated in two murine studies that
333 examined booster immunogenicity in a BNT162b2-experienced immune setting. To
334 approximate the immune background of a vaccinated human population, a vaccine-experienced
335 animal model was generated by vaccinating mice with all licensed BNT162b2 vaccines
336 sequentially spanning 2021 to the present [Original (2-doses), Bivalent Original+BA.4/5 (1-
337 dose), XBB.1.5 (1-dose)]. BNT162b2 XBB.1.5, JN.1, or KP.2-adapted vaccines were
338 administered as a 5th dose to female BALB/c mice 27 days following the XBB.1.5 vaccination
339 (4th dose) (Fig. S4A). Sera were collected prior to and one month following administration of
340 the 5th dose for assessment of pseudovirus neutralization against contemporary JN.1 lineages
341 (JN.1, JN.1.16.1, KP.2, KP.2.3, KP.3, KP.3.1.1, LB.1, and XEC).

342 As a 5th dose, JN.1- and KP.2-adapted vaccines elicited much higher 50% geometric
343 mean neutralizing titers (GMTs) against JN.1 and all JN.1 sublineages tested, as compared to
344 the XBB.1.5 vaccine (Fig. 3A). The JN.1 and KP.2 vaccine responses were 3-to-4 times and 7-
345 to-10 times higher, respectively, compared to the XBB.1.5 vaccine group, including against the
346 globally prevalent KP.3.1.1 sublineage and the rapidly rising XEC sublineage (Fig. 3B). In
347 XBB.1.5 vaccinated animals, neutralizing responses against the antigenically distant JN.1
348 lineage were approximately 20-fold lower than against the vaccine-matched lineage, XBB.1.5
349 (Fig. 3A). In contrast, sera from JN.1- and KP.2-vaccinated mice neutralized all JN.1
350 sublineages with similar potency, indicating a broadly robust and cross-protective immune
351 response. From pre- to post-5th dose, the JN.1-adapted vaccine boosted neutralizing responses
352 (GMT fold rise (GMFR)) against JN.1 and KP.2 by 3.5- and 3.9-fold, respectively. The KP.2-
353 adapted vaccine increased neutralizing responses by 5.9-fold and 7.4-fold against the JN.1 and
354 KP.2 lineages, respectively, as compared to the XBB.1.5 vaccine (Fig. S7). The XBB.1.5-
355 adapted vaccine elicited the lowest GMFRs against JN.1 and KP.2 (0.9 and 1.8, respectively).
356 In a separate study, BNT162b2 XBB.1.5, JN.1, or KP.2 vaccines were administered as a
357 4th dose to female BALB/c mice two weeks after the 3rd dose (BNT162b2 bivalent WT +
358 BA.4/5) (Fig. S4B). As observed in the 5th dose study, sera from JN.1- and KP.2-vaccinated
359 mice neutralized a broad panel of JN.1 sublineages with similar potency (Fig. S8A). Here again,
360 the JN.1- and KP.2-adapted vaccines elicited significantly ($p < 0.05$) higher neutralizing
361 responses against JN.1 sublineages, on the order of 2-to-4-fold and 3-to-7-fold, respectively,
362 than the XBB.1.5 vaccine. GMFRs from pre-to-post 4th dose were also similar between the JN.1
363 and KP.2 vaccines, as compared to the XBB.1.5-adapted vaccine and similar to the magnitude
364 of rise observed when the vaccines were given as a 5th dose (Fig. S8B). Despite the variations in

365 prior vaccination regimens, the JN.1 and KP.2-adapted vaccines elicited consistent
366 neutralization trends and significantly improved immunogenicity against contemporary JN.1
367 lineage pseudoviruses, including against the more recently dominant sublineages (*i.e.*, KP.3.1.1
368 and XEC), as compared to the XBB.1.5 vaccine.
369
370 **BNT162b2 JN.1 and KP.2-adapted vaccines neutralizing responses to JN.1 sublineages in**
371 **naïve mice**
372 The Omicron XBB.1.5, JN.1 and KP.2 vaccines were administered on Days 0 and 21 to naïve
373 female BALB/c mice as a primary series (Fig. S4C). Sera were collected one month after the 2nd
374 dose and tested against the pseudovirus panel used in the vaccine experienced studies described
375 above. Although the BNT162b2 XBB.1.5 vaccine induced robust neutralizing responses against
376 the XBB.1.5 sublineage, it failed to elicit similar neutralizing titers against the antigenically
377 distant JN.1 lineage and sublineages (Fig. 4A). Overall, the JN.1 and KP.2-adapted vaccines
378 elicited significantly higher neutralizing responses against JN.1 and other relevant JN.1
379 sublineages, compared to the XBB.1.5-adapted vaccine (Fig. 4), by an order of magnitude
380 greater than the differences observed in the vaccine-experienced models. Neutralizing GMTs in
381 the JN.1 and KP.2 vaccine groups were 9-to-14-fold and 15-to-29-fold higher against JN.1 and
382 JN.1 sublineages, respectively, as compared to the XBB.1.5 vaccine group (Fig. 4B). Although
383 KP.2-adapted vaccine-elicited GMTs trended 2-to-3-fold higher than JN.1 vaccine-elicited
384 GMTs, these differences were not statistically significant (Fig. 4B).
385
386 **Mapping of neutralizing antibody responses reveals antigenic shifts and drifts of SARS-**
387 **CoV-2 Omicron lineages**

388 To investigate the relative antigenic differences among lineages, as reflected in variant-adapted
389 vaccine humoral immunogenicity, serum neutralizing titers from XBB.1.5-, JN.1- and KP.2-
390 adapted BNT162b2 vaccinated mice (vaccine-experienced and naïve) described above, were
391 used to generate antigenic maps of contemporary SARS-CoV-2 lineages, relative to one another
392 and to the ancestral Wuhan-Hu-1 (WT) strain (Fig. 5). In the map of vaccine-elicited sera from
393 naïve mice, JN.1 and all JN.1-derived sublineages lie within 2 antigenic units (1 unit equals 2-
394 fold change in neutralization titer) from each other, suggesting a high antigenic similarity and
395 indicative of limited antigenic drift within the JN.1 cluster thus far (Fig. 5A). In contrast, JN.1
396 and JN.1-derived sublineages were found to lie more than 4 antigenic units away from the
397 original WT strain, and previously dominant lineages BA.4/5 and Omicron XBB.1.5, indicating
398 a major antigenic shift from earlier SARS-CoV-2 lineages. Sera from vaccine-experienced mice
399 yielded similar spatial relationships (Fig. 5B); however, these data are likely confounded by the
400 influence of cross-reactive antibodies recognizing conserved epitopes. Antigenic maps
401 generated in a naïve background more accurately reflect the true antigenic differences between
402 virus strains or species. The cartographies of both backgrounds, however, clearly demonstrate
403 that evolution toward JN.1 lineages marks a major antigenic shift from prior dominant lineages,
404 such as those belonging to the XBB cluster. The distance of JN.1 lineages from XBB.1.5 is even
405 greater than the latter is from its epidemiologically dominant predecessor, BA.4/5. However, the
406 JN.1 lineages, particularly the parental JN.1 and its derivative KP.2, occupy proximal or
407 overlapping coordinates of the antigenic maps, which is consistent with the similarity in
408 neutralizing activity elicited by both vaccines against the entire panel of JN.1 sublineages.
409

410 **BNT162b2 JN.1- and KP.2-adapted vaccines induce comparable S-specific $CD4^+$ and**
411 **$CD8^+$ T cell responses in BNT162b2-experienced and naïve mice**

412 In both vaccine-experienced and naïve mice, spleens collected one-month following final
413 vaccination were interrogated for S-specific T cell cytokine responses using a flow cytometry-
414 based intracellular cytokine staining (ICS) assay (Fig. S6). Peptide pools representing the full-
415 length S protein from the Wuhan (WT) virus, BA.4/5, XBB.1.5, JN.1 and KP.2 variants were
416 used to assess lineage-specific $CD4^+$ and $CD8^+$ T cell responses *ex vivo*.

417 In vaccine-experienced mice, the XBB.1.5, JN.1 and KP.2 vaccines induced overall high
418 frequencies of S-specific $CD4^+$ and $CD8^+$ T cells as compared to the saline control (Fig. 6, Fig.
419 S9). Mice administered the 5th dose (Fig. S4A) of KP.2 or JN.1-adapted vaccine elicited similar
420 frequencies of IFN-γ^+, TNF-α^+, and IL-2^+ $CD4^+$ T cells, as compared to the XBB.1.5 vaccine
421 (Fig. 6A-C). Within each vaccine group the frequencies of cytokine expressing $CD4^+$ T cells
422 were similar across all the lineages tested, indicating that the T cell responses were highly cross-
423 reactive. Similarly, for the cytokine expressing (IFN-γ^+ or TNF-α^+ or IL-2^+) $CD8^+$ T cells, the
424 KP.2 and JN.1-adapted vaccine elicited comparable frequencies as the XBB.1.5-adapted
425 vaccine (Fig. 6D-F). Within each vaccine group, individual lineage-specific T cell frequencies
426 varied slightly; however, these variations did not impact the overall magnitude of the T cell
427 response, and each vaccine was capable of inducing robust T cell cytokine responses against all
428 the lineages analyzed. The same was true for polyfunctional (IFN-γ^+ TNF-α^+ IL-2^+) $CD4^+$ (Fig.
429 S9A) and $CD8^+$ T cells (Fig. S9B).

430 In naïve mice, the trends for both $CD4^+$ (Fig. 7A-C, Fig. S10A) and $CD8^+$ (Fig. 7D-F,
431 Fig. S10B) T cell responses elicited by the JN.1 and KP.2 vaccines, with respect to cross-
432 reactivity and similarity to one another and to the XBB.1.5 vaccine, were generally consistent

433 with those observed in the vaccine-experienced study. In both models, minimal IL-4 secreting
434 $CD4^+$ T cells were detected (data not shown), particularly in relation to those secreting IFN-γ,
435 TNF-α and IL-2, indicating a strong bias toward a Th1 over a Th2 cytokine profile, consistent
436 with character of the T cell responses elicited by the original and earlier versions of BNT162b2
437 [23,25].
438
439 **DISCUSSION**
440 The dynamic epidemiologic landscape of SARS-CoV-2 presents a unique challenge for
441 the development of periodically updated COVID-19 vaccines. Since its emergence, SARS-
442 CoV-2 has evolved quickly and broadly, comparable to other respiratory viruses that account
443 for a large burden of disease, such as influenza [29]. The periodicity of disease incidence, though,
444 has not aligned with the more predictable seasonality of other respiratory viral infections [30,31].
445 These attributes pose challenges for vaccine manufacturers and regulatory authorities alike in
446 making decisions about what lineages to target in vaccine updates and when to introduce those
447 updated vaccines into the general population, to make the greatest impact in reducing the
448 burden of COVID-19 morbidity and mortality.
449 The FDA recently approved the 2024-2025 formula of BNT162b2 for individuals 12
450 years of age and older and granted emergency use authorization (EUA) for individuals 6 months
451 through 11 years of age in the US [32], following a recommendation to mRNA vaccine
452 manufacturers to target the KP.2 lineage in the vaccine update [11]. The genetic drift of lineages,
453 and questions around the relative antigenic proximity to future lineages that may emerge in the
454 Northern Hemisphere Winter of 2024/2025, has prompted slightly different recommendations
455 from regulatory authorities on the composition of a vaccine update [9-11]. As such, both JN.1- and

456 KP.2-adapted formulas of the BNT162b2 vaccine have been approved and authorized in
457 different countries. The nonclinical evaluation of both formulas in multiple immune
458 backgrounds against a broad panel of immunologically and epidemiologically relevant
459 contemporary lineages, summarized here, has enabled an informed decision-making process in
460 the development of these variant-adapted vaccines.

461 JN.1 differs from most of its descendant lineages by 1 to 5 amino acid residues in the S
462 protein, which is in the same range of difference that separated XBB.1.5 from other dominant
463 XBB sublineages [33]. As the XBB.1.5 vaccine conferred cross-protective immunity against other
464 sublineages within the XBB lineage cluster [15-19,34], we hypothesized that JN.1 and KP.2-adapted
465 vaccines would be similarly effective in generating broad immune responses against
466 contemporary JN.1 sublineages. Virus neutralizing antibody responses trend closely with
467 protection from COVID-19 disease [20,35,36], and therefore have been a useful surrogate for
468 COVID-19 vaccine performance against emerging lineages. The degree to which those lineages
469 escape vaccine elicited neutralization has generally served as a metric of how well updated
470 vaccines will protect against COVID-19.

471 To elucidate potential molecular mechanisms of immune escape, we sought to first
472 characterize the JN.1 and KP.2 full-length prefusion stabilized S(P2) proteins and RBDs. Our
473 data revealed the unique molecular features of JN.1 and KP.2 S(P2) gained from the extensive
474 mutations during viral evolution. The S(P2) proteins of both JN.1 and KP.2 have lower T_m as
475 compared to the WT and XBB.1.5 S(P2) proteins [23]. This finding is consistent with the idea that
476 SARS-CoV-2 may be evolving toward gradually reduced thermostability, which, along with the
477 increased population of S in RBD-up conformations, could contribute to increased infectivity and
478 transmissibility, and account for the epidemiologic growth advantage of these lineages relative to

479 their predecessors. When assessing ACE2 binding affinity of the new JN.1 lineages, the RBDs of
480 JN.1 and KP.2 have inherited several mutations also contained in XBB.1.5 that enhance receptor
481 binding, such as G446S, Q498R, N501Y and Y505H in the RBM. The additional E484K
482 substitution acquired by JN.1 and KP.2 may contribute to further enhancement of receptor binding
483 via a salt bridge with E35 from ACE2 (Fig. 1D). This likelihood is supported by data that shows
484 JN.1 and KP.2 RBD bind to ACE2 with a higher potency, as compared to the WT RBD[23].

485 Few cryo-EM structures of SARS-CoV-2 S proteins have been resolved with more than
486 one RBD-up conformation and not bound to ACE2 or antibodies [37]. KP.2 exhibits a greater
487 propensity to occupy the RBD-up conformation than does JN.1, despite these lineages differing
488 at only three residues in the S protein. We reason that inter-RBD interactions conferred by
489 F456L substitution may stabilize the RBD up conformation. In the 1- and 2-up KP.2 structures,
490 L456 of the down-RBD is in the immediate vicinity of P384 of the up-RBD, and likely
491 participates in hydrophobic interactions (Fig. 2D, Fig. S3). The FPPR is only well-resolved in
492 the protomer bearing the up conformation in the 1-up structures. The improved resolution of
493 this feature in the KP.2 versus the JN.1 structure may be due in part to the stabilization imposed
494 by the inter-RBD contact mediated by L456, especially as RBD dynamics have been implicated
495 in interactions within this distal region [38,39].

496 Previous non-prefusion-stabilized structures of the Omicron BA.1 lineage revealed that
497 the 630-loop was well resolved in the down conformation [40], like the D614G and other earlier
498 lineages [38,39]. The P612S mutation may play a role similar to D614G by stabilizing the FPPR via
499 a structured 630-loop, thereby enhancing the stability of the cleaved trimer and bolstering
500 interactions between protomers, as well as between S1 and S2; however, doing so in the setting
501 of the up conformation, like the Gamma variant [38].

502 The P1143 residue is located at the N-terminus of the stem helix. The secondary amide
503 between the side chain and the main chain renders this residue unable to donate an upstream
504 hydrogen bond. Conversely, L1143, a new mutation acquired by both JN.1 and KP.2 can
505 capitalize on this hydrogen bonding interaction, where this additional secondary structure is likely
506 to enforce an alternative trajectory of the stem helix. The interior facing residues of the stem are
507 the target of weak, broadly neutralizing antibodies and the P1443L mutation may, therefore,
508 represent an initial step toward stabilizing a conformation of the stem helix that occludes this
509 epitope, yet is not detrimental to attaining the postfusion conformation.

510 Neutralizing antibodies that are overrepresented at the population level are key drivers of
511 antigenic drift, as most that have conserved gene usage and stereotyped epitope recognition have
512 been rendered ineffective by point mutations [41]. For example, P4J15 is a rare antibody that
513 recognizes the class 1 epitope and has maintained breadth from the original Wuhan strain through
514 XBB.1 [42]. However, the F456L mutation, present in KP.2 and located within the P4J15 epitope,
515 likely impacts its binding (Fig. 2E). The N364 glycan is similarly located in a region recognized
516 by broadly neutralizing antibodies, such as G32R7 (Fig. 2E). This region is known as the RBD
517 class 3 or the RBD1 competition cluster, and represents the largest memory B cell epitope cluster
518 among convalescent patients infected at the start of the pandemic [28]. The mutations found in KP.2
519 likely perturb the epitopes of the few remaining neutralizing antibodies elicited by the Wuhan
520 strain and underpin much of its fitness and immune escape among the SARS-CoV-2-experienced
521 population.

522 As nonclinical data have closely aligned with clinical responses in prior cycles of variant-
523 adapted vaccine updates [14], we assessed the immunogenicity of BNT162b2 JN.1 and KP.2
524 vaccines against JN.1 and contemporary circulating sublineages of epidemiologic relevance in

525 BNT162b2-experienced and naïve mice. As most adults have developed hybrid immunity from a
526 mixture of prior infections and vaccinations, recapitulating the collective history of antigenic
527 exposures has become an increasingly complex endeavor, particularly with the successive
528 emergence of new lineage clusters each year . Nonetheless, models that account for prior exposure
529 history provide a more relevant model for evaluating vaccine responses in immune experienced
530 populations. To understand the impact of varying immune backgrounds on variant-adapted
531 vaccine immunogenicity, we assessed vaccine-elicited immune responses in studies with differing
532 compositions and schedules of prior vaccinations. The most parsimonious model that maintains
533 immunologic relevance is likely to streamline preparatory activities for future vaccine updates.

534 Prior preclinical data that supported FDA approval of the BNT162b2 XBB.1.5 vaccine in
535 2023 showed that vaccine-elicited neutralizing responses against the vaccine-matched XBB.1.5
536 and related lineages (*e.g*. XBB.1.16, XBB.2.3) were 4-to-5 times higher than responses elicited
537 against the same lineage by the previously authorized vaccine (bivalent WT + Omicron BA.4/5)
538 [23]. Similarly, in the present studies, JN.1 and KP.2-adapted vaccines, elicited neutralizing titers
539 against JN.1 sublineages that were consistently improved over BNT162b2 XBB.1.5 vaccine
540 responses. Overall, there was a 3-to-10-fold improved response over the XBB.1.5 vaccine in
541 BNT162b2-experienced mice across two studies, depending on the vaccine formulation and the
542 sublineage tested. JN.1 and KP.2 vaccines both elicited responses that effectively neutralized all
543 16 JN.1 pseudoviruses evaluated, including those sublineages that acquired advantageous R346T
544 and F456L substitutions (*e.g.*, JN.1.16.1, KP.2), and a next generation of sublineages that have
545 an additional advantageous deletion at the S31 position (*e.g.*, KP.2.3, LB.1) [43]. KP.3 and its most
546 dominant KP.3.1.1 sublineage, as well as the rapidly emerging recombinant XEC lineage [13], were
547 also evaluated and neutralized by JN.1 and KP.2 vaccines in the studies reported here.

548 As multiple animal models are employed in the evaluation of COVID-19 vaccines,
549 many still frequently perform primary series studies in naïve animals [44-48], which does not
550 account for the current immune experience of most adults. Even when vaccine-experienced
551 animal studies are employed to better recapitulate the antigenic exposures of the general
552 population, there remains a lack of consensus on how those studies should be designed. To
553 inform investigations into the influence of varied immune backgrounds, we assessed JN.1 and
554 KP.2 vaccine immunogenicity against two different vaccine-experience regimens, varying the
555 prior vaccine composition and schedule. Across both studies, we observed a similar trend in
556 neutralizing antibody responses for both JN.1 and KP.2 vaccines, regardless of prior BNT162b2
557 XBB.1.5 vaccine exposure or timing between vaccine administrations. Mice boosted with JN.1
558 or KP.2-adapted vaccines as a 4th dose elicited greater immunity against JN.1 and a broader
559 panel of JN.1 sublineages, consistent with findings of the 5th dose study. These findings indicate
560 that the exact sequence and scheme of prior antigenic exposures may not affect trends in
561 responses elicited by variant-updated vaccines. It may be more important to reproduce
562 exposures with the ancestral strain and an Omicron lineage as a means to approximate the
563 immune experience of the general population.

564 Despite the importance of immune-experienced models, it is critical to also evaluate
565 vaccine immunogenicity in naïve models that are particularly relevant to younger age cohorts
566 that have not yet been exposed to SARS-CoV-2 through either infection or vaccination.
567 Children under the age of four experience a high burden of COVID-19 hospitalization. During
568 the 2023–2024 respiratory season in the US, the cumulative COVID-19 hospitalization rate for
569 children under four was 104.3 per 100,000, and was higher only among persons ≥50 years of
570 age [4]. Notably, 50% of infants, children, and adolescents ≤17 years hospitalized with COVID-

571 19 from July 2023–March 2024, and 40% of those admitted to the ICU, had no underlying
572 medical conditions [49]. According to 2023 data in the US, COVID-19 was the third leading cause
573 of death due to infectious disease in individuals 0–17 years of age [50]. Given this public health
574 relevance, we evaluated a two-dose primary series in naïve mice, wherein we found that both
575 JN.1 and KP.2-adapted vaccines elicited a similar breadth of neutralizing activity against all
576 JN.1 sublineages that were improved over the XBB.1.5 vaccine responses by an order of
577 magnitude (8-to-29-fold higher). Responses elicited by the XBB.1.5 vaccine were also higher
578 (10-fold) than the prior vaccine (bivalent WT + Omicron BA.4/5) in a previous study [23].
579 Although the comparative trends in neutralizing responses across vaccine groups were
580 consistent across vaccine-experienced and naïve mouse studies, the magnitude of those
581 differences were much greater in the naïve model, reflecting the considerable antigenic distance
582 between the XBB and JN.1 lineage clusters.

583 Overall, JN.1 and KP.2 BNT162b2 vaccines elicited improved neutralizing
584 antibody responses over the XBB.1.5 vaccine in mice against the contemporary JN.1
585 lineages. Additionally, the maintenance of comparable T cell responses between
586 vaccines across a broad set of variant-specific peptides in mice after booster vaccination
587 indicates that cellular immune responses are not substantially impacted by the
588 mutational differences among recent Omicron lineages. Biophysical characterization
589 indicated that JN.1 and KP.2 S proteins are relatively similar to one another but differ in
590 their structural features from prior Omicron lineages. As XBB.1.5 vaccines have
591 demonstrated diminished effectiveness against the JN.1 lineage cluster, and preclinical
592 data have trended closely with clinical responses and real-world effectiveness outcomes,
593 it is anticipated that the potent responses elicited by both the JN.1 and KP.2-adapted

594 BNT162b2 vaccines will confer robust protection against antigenically drifted JN.1 sublineages,
595 including the most globally dominant and recently rising strains, similar to how the XBB.1.5
596 vaccine performed against the XBB lineage cluster [16-18,34]. As reported here, and moving
597 forward into the current and future peak seasons of COVID-19 disease activity, a
598 multidimensional approach is needed to monitor the evolutionary dynamics and epidemiology
599 of novel SARS-CoV-2 lineages and the effectiveness of the JN.1- and KP.2-adapted vaccines in
600 protecting against a wide range of clinical outcomes.
601

602 **Acknowledgements**
603 We thank the Pfizer Comparative Medicine department and veterinary staff at Pearl River, NY
604 for their contributions to the *in vivo* studies; members of Pfizer Vaccine Research and
605 Development at Pearl River, NY, for their contributions to assay development and
606 implementation, virus variant monitoring, material production and characterization, and
607 material and technical support in molecular biology, virology and immunology; and members of
608 Pfizer Discovery Sciences in Groton, CT, for their material and technical support on
609 recombinant protein production and characterization. The authors also thank Teresa Hauguel for
610 review of the manuscript, Christina D'Arco for writing and graphics support and Charlotte Ford
611 for editorial assistance.
612

613 **Funding**
614 This study was supported by Pfizer.
615

616 **Author Contributions**

617 WC contributed to writing of the original draft, methodology, investigation, and data generation
618 and interpretation. KRT contributed to the writing of the original draft, investigation, data
619 generation and interpretation. IWW contributed to writing of the original draft, cryo-EM
620 structural determination and visualization, data analysis and interpretation. LTM, MR, WL, SS,
621 SR, KPD, AY, DS, SM, SS, WS, RMM and PMD contributed to data generation, analysis,
622 visualization and interpretation; LTM also contributed to serologic methodology. JSC
623 performed antigen purification and thermal shift experiments. PS performed BLI experiments.
624 KFF performed recombinant protein expression. TJM and GMW performed site-specific glycan
625 mapping by MS studies. APM contributed to data analysis. CIC and AM contributed to data
626 interpretation. US and ASA supervised the work. HW contributed to writing of the original
627 draft, supervision, investigation, visualization, data interpretation and analysis related to the
628 structural and biophysical work. KAS contributed to writing of the original draft, data
629 interpretation, investigation, and overall supervision and conceptualization of the work. KM
630 contributed to writing of the original draft, experimental designs, data analysis and
631 interpretation, investigation and overall supervision and conceptualization of the work. All
632 authors contributed to the development and critical review of the manuscript and have read and
633 agreed to the published version.
634
635 **Competing Interests**
636 All authors are current or former employees of Pfizer or BioNTech and may, therefore, be
637 respective shareholders. Pfizer and BioNTech participated in the design, analysis and
638 interpretation of the data as well as the writing of this report and the decision to publish. WL,
639 AM, UŞ, KAS and KM are inventors on patents and patent applications related to the COVID-

640 19 vaccine. AM and UŞ are inventors on patents and patent applications related to RNA

641 technology.

642

643 **References**

644 1 HHS. *COVID-19 Reported Patient Impact and Hospital Capacity by State Timeseries*
645 *(RAW)*, <https://healthdata.gov/Hospital/COVID-19-Reported-Patient-Impact-and-
646 Hospital-Capa/g62h-syeh/about_data> (2024).
647 2 CDC. *Disease Burden of Flu*, <https://www.cdc.gov/flu/about/burden/> (2023).
648 3 CDC. *Preliminary Estimated Flu Disease Burden 2023–2024 Flu Season*,
649 <https://www.cdc.gov/flu-burden/php/data-vis/2023-2024.html> (2024).
650 4 CDC. *COVID Data Tracker*, <https://covid.cdc.gov/covid-data-tracker/#datatracker-
651 home> (2024).
652 5 corneliusroemer. *cov-lineages / pango-designation*, <https://github.com/cov-
653 lineages/pango-designation/blob/master/lineage_notes.txt> (2024).
654 6 FDA. *Vaccines and Related Biological Products Advisory Committee June 5, 2024*
655 *Meeting Announcement*, <https://www.fda.gov/advisory-committees/advisory-
656 committee-calendar/vaccines-and-related-biological-products-advisory-committee-
657 june-5-2024-meeting-
658 announcement#:~:text=On%20June%205%2C%202024%2C%20the,and%2For%20video
659 %20conferencing%20platform.> (2024).
660 7 FDA. *Vaccines and Related Biological Products Advisory Committee June 15, 2023*
661 *Meeting Announcement*, <https://www.fda.gov/advisory-committees/advisory-
662 committee-calendar/vaccines-and-related-biological-products-advisory-committee-
663 june-15-2023-meeting-announcement> (2023).
664 8 FDA. *Vaccines and Related Biological Products Advisory Committee June 28, 2022*
665 *Meeting Announcement*, <https://www.fda.gov/advisory-committees/advisory-
666 committee-calendar/vaccines-and-related-biological-products-advisory-committee-
667 june-28-2022-meeting-announcement> (2022).
668 9 W.H.O. *Statement on the antigen composition of COVID-19 vaccines*,
669 <https://www.who.int/news/item/26-04-2024-statement-on-the-antigen-composition-
670 of-covid-19-vaccines> (2024).
671 10 EMA. *ETF recommends updating COVID-19 vaccines to target new JN.1 variant*,
672 <https://www.ema.europa.eu/en/news/etf-recommends-updating-covid-19-vaccines-
673 target-new-jn1-variant> (2024).
674 11 FDA. *Updated COVID-19 Vaccines for Use in the United States Beginning in Fall 2024*,
675 <https://www.fda.gov/vaccines-blood-biologics/updated-covid-19-vaccines-use-
676 united-states-beginning-fall-2024> (2024).
677 12 W.H.O. *Initial risk evaluation of JN.1, 19 December 2023*,
678 <https://www.who.int/docs/default-
679 source/coronaviruse/18122023_jn.1_ire_clean.pdf> (2023).

680 13 W.H.O. *COVID-19 epidemiological update – 9 October 2024*,
681 <https://www.who.int/publications/m/item/covid-19-epidemiological-update-edition-
682 172> (2024).
683 14 Gayed, J. *et al.* Immunogenicity of the Monovalent Omicron XBB.1.5-Adapted
684 BNT162b2 COVID-19 Vaccine against XBB.1.5, BA.2.86, and JN.1 Sublineages: A Phase
685 2/3 Trial. *Vaccines (Basel)* **12** (2024). https://doi.org:10.3390/vaccines12070734
686 15 Gayed, J. *et al.* Safety and Immunogenicity of the Monovalent Omicron XBB.1.5-
687 Adapted BNT162b2 COVID-19 Vaccine in Individuals >/=12 Years Old: A Phase 2/3 Trial.
688 *Vaccines (Basel)* **12** (2024). https://doi.org:10.3390/vaccines12020118
689 16 Wang, Q. *et al.* XBB.1.5 monovalent mRNA vaccine booster elicits robust neutralizing
690 antibodies against XBB subvariants and JN.1. *Cell Host Microbe* **32**, 315-321 e313
691 (2024). https://doi.org:10.1016/j.chom.2024.01.014
692 17 Wang, Q. *et al.* Robust SARS-CoV-2-neutralizing antibodies sustained through 6 months
693 post XBB.1.5 mRNA vaccine booster. *Cell Rep Med* **5**, 101701 (2024).
694 https://doi.org:10.1016/j.xcrm.2024.101701
695 18 Tartof, S. Y. *et al.* Effectiveness of BNT162b2 XBB Vaccine Against XBB and JN.1
696 Sublineages. *Open Forum Infect Dis* **11**, ofae370 (2024).
697 https://doi.org:10.1093/ofid/ofae370
698 19 Ma, K. C. *et al.* Effectiveness of Updated 2023-2024 (Monovalent XBB.1.5) COVID-19
699 Vaccination Against SARS-CoV-2 Omicron XBB and BA.2.86/JN.1 Lineage Hospitalization
700 and a Comparison of Clinical Severity-IVY Network, 26 Hospitals, October 18, 2023-
701 March 9, 2024. *Clin Infect Dis* (2024). https://doi.org:10.1093/cid/ciae405
702 20 Khoury, D. S. *et al.* Neutralizing antibody levels are highly predictive of immune
703 protection from symptomatic SARS-CoV-2 infection. *Nat Med* **27**, 1205-1211 (2021).
704 https://doi.org:10.1038/s41591-021-01377-8
705 21 Kaku, Y. *et al.* Virological characteristics of the SARS-CoV-2 KP.2 variant. *Lancet Infect*
706 *Dis* **24**, e416 (2024). https://doi.org:10.1016/S1473-3099(24)00298-6
707 22 W.H.O. *Interim statement on hybrid immunity and increasing population*
708 *seroprevalence rates*, <https://www.who.int/news/item/01-06-2022-interim-
709 statement-on-hybrid-immunity-and-increasing-population-seroprevalence-rates>
710 (2022).
711 23 Modjarrad, K. *et al.* Preclinical Characterization of the Omicron XBB.1.5-Adapted
712 BNT162b2 COVID-19 Vaccine. *bioRxiv* **accepted in Npj Vaccines**,
713 2023.2011.2017.567633 (2023). https://doi.org:10.1101/2023.11.17.567633
714 24 Shajahan, A., Pepi, L. E., Kumar, B., Murray, N. B. & Azadi, P. Site specific N- and O-
715 glycosylation mapping of the spike proteins of SARS-CoV-2 variants of concern. *Sci Rep*
716 **13**, 10053 (2023). https://doi.org:10.1038/s41598-023-33088-0
717 25 Vogel, A. B. *et al.* BNT162b vaccines protect rhesus macaques from SARS-CoV-2. *Nature*
718 **592**, 283-289 (2021). https://doi.org:10.1038/s41586-021-03275-y
719 26 Liu, P. *et al.* Spike N354 glycosylation augments SARS-CoV-2 fitness for human
720 adaptation through structural plasticity. *Natl Sci Rev* **11**, nwae206 (2024).
721 https://doi.org:10.1093/nsr/nwae206

722 27 Li, L. *et al.* Spike structures, receptor binding, and immune escape of recently
723 circulating SARS-CoV-2 Omicron BA.2.86, JN.1, EG.5, EG.5.1, and HV.1 sub-variants.
724 *Structure* **32**, 1055-1067 e1056 (2024). https://doi.org:10.1016/j.str.2024.06.012
725 28 Tong, P. *et al.* Memory B cell repertoire for recognition of evolving SARS-CoV-2 spike.
726 *Cell* **184**, 4969-4980 e4915 (2021). https://doi.org:10.1016/j.cell.2021.07.025
727 29 Wang, X. *et al.* SARS-CoV-2 versus Influenza A Virus: Characteristics and Co-Treatments.
728 *Microorganisms* **11** (2023). https://doi.org:10.3390/microorganisms11030580
729 30 Gong, Z. *et al.* Natural and socio-environmental factors in the transmission of COVID-
730 19: a comprehensive analysis of epidemiology and mechanisms. *BMC Public Health* **24**,
731 2196 (2024). https://doi.org:10.1186/s12889-024-19749-3
732 31 Barosa, M., Ioannidis, J. P. A. & Prasad, V. Evidence base for yearly respiratory virus
733 vaccines: Current status and proposed improved strategies. *Eur J Clin Invest*, e14286
734 (2024). https://doi.org:10.1111/eci.14286
735 32 FDA. *Pfizer-BioNTech COVID-19 Vaccine: Pfizer-BioNTech COVID-19 Vaccine (2024-2025*
736 *Formula) Authorized For Individuals 6 Months through 11 Years of Age*,
737 <https://www.fda.gov/vaccines-blood-biologics/coronavirus-covid-19-cber-regulated-
738 biologics/pfizer-biontech-covid-19-vaccine> (2024).
739 33 Tamura, T. *et al.* Virological characteristics of the SARS-CoV-2 Omicron XBB.1.5 variant.
740 *Nat Commun* **15**, 1176 (2024). https://doi.org:10.1038/s41467-024-45274-3
741 34 Chalkias, S. *et al.* Interim Report of the Reactogenicity and Immunogenicity of Severe
742 Acute Respiratory Syndrome Coronavirus 2 XBB-Containing Vaccines. *The Journal of*
743 *infectious diseases* **230**, e279-e286 (2024). https://doi.org:10.1093/infdis/jiae067
744 35 Cromer, D. *et al.* Neutralising antibody titres as predictors of protection against SARS-
745 CoV-2 variants and the impact of boosting: a meta-analysis. *Lancet Microbe* **3**, e52-e61
746 (2022). https://doi.org:10.1016/S2666-5247(21)00267-6
747 36 Earle, K. A. *et al.* Evidence for antibody as a protective correlate for COVID-19 vaccines.
748 *Vaccine* **39**, 4423-4428 (2021). https://doi.org:10.1016/j.vaccine.2021.05.063
749 37 Cai, Y. *et al.* Structural basis for enhanced infectivity and immune evasion of SARS-CoV-
750 2 variants. *Science* **373**, 642-648 (2021). https://doi.org:10.1126/science.abi9745
751 38 Zhang, J. *et al.* Membrane fusion and immune evasion by the spike protein of SARS-
752 CoV-2 Delta variant. *Science* **374**, 1353-1360 (2021).
753 https://doi.org:10.1126/science.abl9463
754 39 Zhang, J. *et al.* Structural impact on SARS-CoV-2 spike protein by D614G substitution.
755 *Science* **372**, 525-530 (2021). https://doi.org:10.1126/science.abf2303
756 40 Zhang, J. *et al.* Structural and functional impact by SARS-CoV-2 Omicron spike
757 mutations. *Cell Rep* **39**, 110729 (2022). https://doi.org:10.1016/j.celrep.2022.110729
758 41 Cao, Y. *et al.* Omicron escapes the majority of existing SARS-CoV-2 neutralizing
759 antibodies. *Nature* **602**, 657-663 (2022). https://doi.org:10.1038/s41586-021-04385-3
760 42 Fenwick, C. *et al.* Broadly potent anti-SARS-CoV-2 antibody shares 93% of epitope with
761 ACE2 and provides full protection in monkeys. *J Infect* **87**, 524-537 (2023).
762 https://doi.org:10.1016/j.jinf.2023.10.008
763 43 Li, P. *et al.* Neutralization and Stability of JN.1-derived LB.1, KP.2.3, KP.3 and KP.3.1.1
764 Subvariants. *bioRxiv* (2024). https://doi.org:10.1101/2024.09.04.611219

765 44 Slamanig, S. *et al.* Intranasal SARS-CoV-2 Omicron variant vaccines elicit humoral and
766 cellular mucosal immunity in female mice. *EBioMedicine* **105**, 105185 (2024).
767 https://doi.org:10.1016/j.ebiom.2024.105185
768 45 Zhang, Y. *et al.* Three SARS-CoV-2 spike protein variants delivered intranasally by
769 measles and mumps vaccines are broadly protective. *Nat Commun* **15**, 5589 (2024).
770 https://doi.org:10.1038/s41467-024-49443-2
771 46 Yang, Z. H. *et al.* Measles Virus-Based Vaccine Expressing Membrane-Anchored Spike of
772 SARS-CoV-2 Inducing Efficacious Systemic and Mucosal Humoral Immunity in Hamsters.
773 *Viruses* **16** (2024). https://doi.org:10.3390/v16040559
774 47 Hoffmann, M. A. G. *et al.* ESCRT recruitment to SARS-CoV-2 spike induces virus-like
775 particles that improve mRNA vaccines. *Cell* **186**, 2380-2391 e2389 (2023).
776 https://doi.org:10.1016/j.cell.2023.04.024
777 48 Singh, O. N. *et al.* Immunogenicity and protection efficacy of self-amplifying and
778 circular mRNA vaccines for SARS-CoV-2. *bioRxiv*, 2024.2008.2023.609366 (2024).
779 https://doi.org:10.1101/2024.08.23.609366
780 49 Havers, F. P. *COVID-19–Associated Hospitalizations among Children and Adults —*
781 *COVID-NET*, <https://www.cdc.gov/acip/downloads/slides-2024-06-26-28/02-COVID-
782 Havers-508.pdf> (2024).
783 50 CDC. *About Provisional Mortality Statistics, 2018 through Last Week*,
784 <https://wonder.cdc.gov/mcd-icd10-provisional.html> (

785

786

787

788

789

790

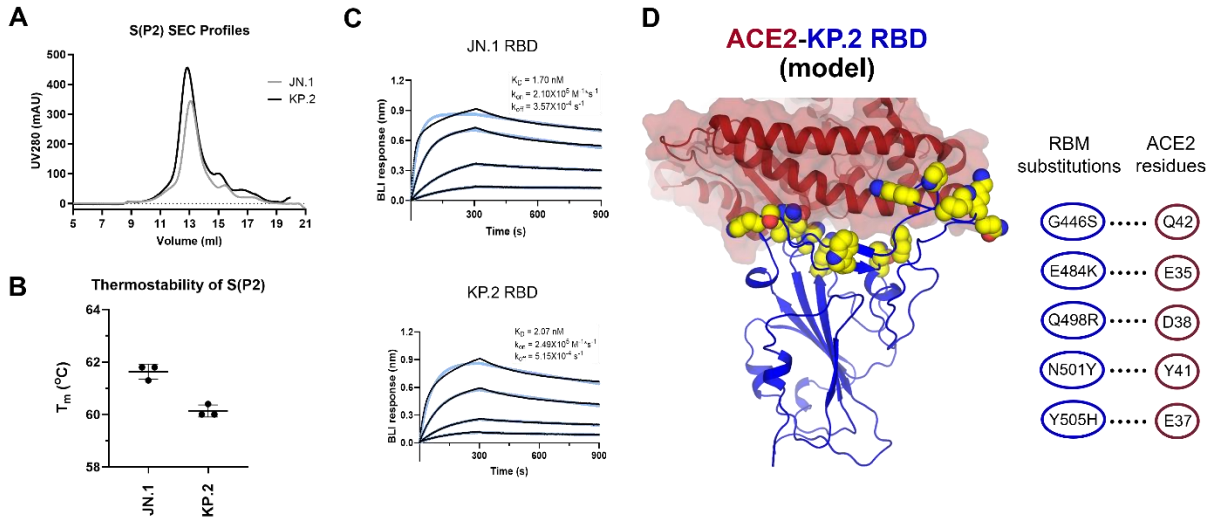

Figure 1. Biophysical Characteristics of SARS-CoV-2 Omicron JN.1 and KP.2 Prefusion-Stabilized Spike and Receptor Binding Domain. a SEC profiles of the S(P2) proteins of JN.1 and KP.2. The S(P2) proteins were purified in DDM (*n*-dodecyl-*β*-D-maltopyranoside, see Supplementary Materials). SDS-PAGE fractions from 12 mL to 15 mL of each FL S construct are shown in Fig. S1B. **b** Melting temperature (Tm) of purified S(P2) proteins determined by the inflection point of the first derivatives of protein fluorescence signals collected at 330 nm over that of 350 nm. Experiments were conducted by Tycho NT.6 and run in triplicates (n=3). **c** Biolayer interferometry (BLI) sensorgrams of RBD binding to immobilized human angiotensin converting enzyme-2 peptidase domain (ACE2-PD). The binding curves (black) were globally fit to a 1:1 Langmuir binding model (light blue). Calculated apparent K_D, k_{on}, k_{off} values are listed in the figure. **d** Crystal structure of ACE2-PD (PDB: 6M0J) is aligned to the KP.2 1-up RBD. ACE2-PD is shown in maroon ribbon with surface representation. KP.2 RBD is shown in blue cartoon with amino acid residue changes in the receptor binding motif (RBM) from WT to KP.2 shown in yellow spheres. RBM residue changes (blue circle) that enhance receptor binding via putative specific interactions (dotted lines) to ACE2 residues (maroon circle) are shown in the interaction scheme on the right.

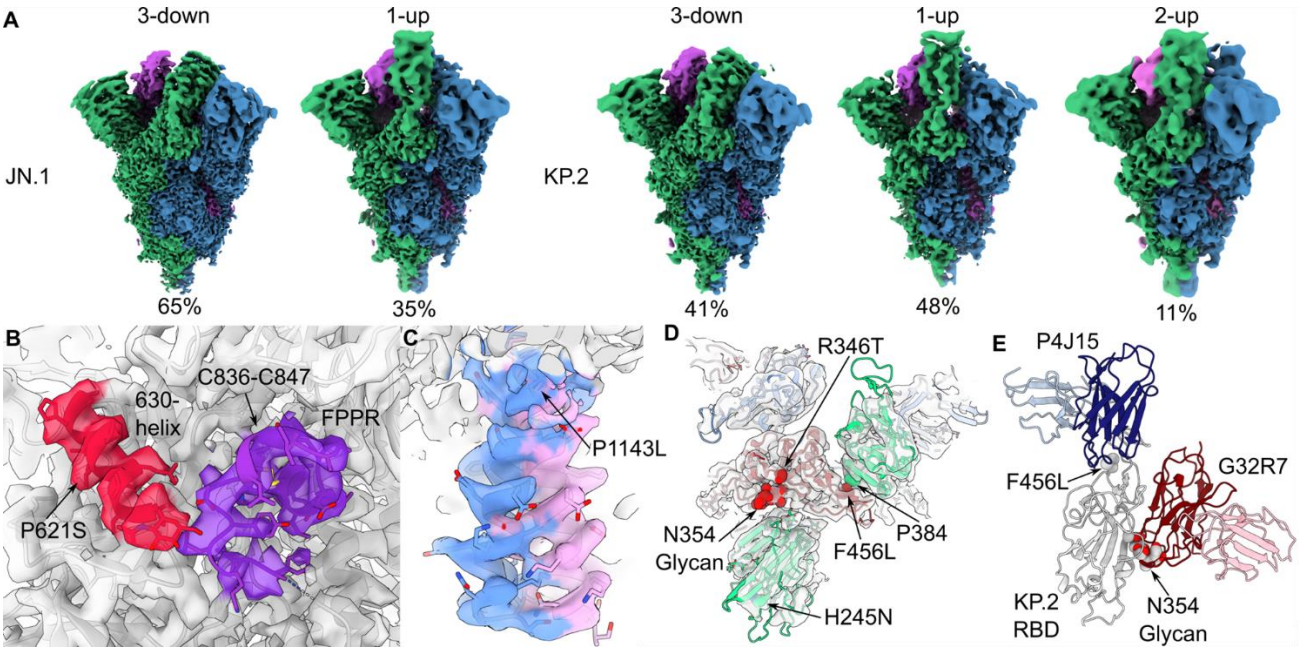

Figure 2. Structural and Functional Consequences of SARS-CoV-2 JN.1 and KP.2 S Protein Mutations. a Local resolution-filtered maps of the final 3D reconstructions are shown for each of the resolved RBD conformational states and colored by protomer. Local resolution estimations for maps shown in panels A though D are found in Figure S3. The first up RBD is colored green in both the JN.1 and KP.2 maps and the second up RBD in the KP.2 is colored blue. Proportions of particles derived from reference-based classification are expressed as a percentage below each map. **b** Magnified view of the 630-helix and fusion peptide proximal region (FPPR) from the KP.2 1-RBD-up map overlaid with the model shows the quality of the EM density in this region. **c** Magnified view of the stem from the JN.1 3-RBD-down map overlaid with the model shows the two partially occupied conformations of this helix beginning at the P1143L mutation. **d** Top view of the KP.2 1-RBD-up conformation structure shows the location of the N354 glycan due to the K356T substitution and a putative interprotomer hydrophobic interaction with P384 due to the F456L substitution. **e** Broad monoclonal antibodies (mAbs) G32R7 (PDB: 7N65) and P4J15 (PDB: 8PQ2), which bind early omicron lineages, are aligned to the KP.2 1-RBD-up. The proximity of these epitopes and the K356T and F456L substitution-induced surface alterations implicate these changes with evasion of early immunity.

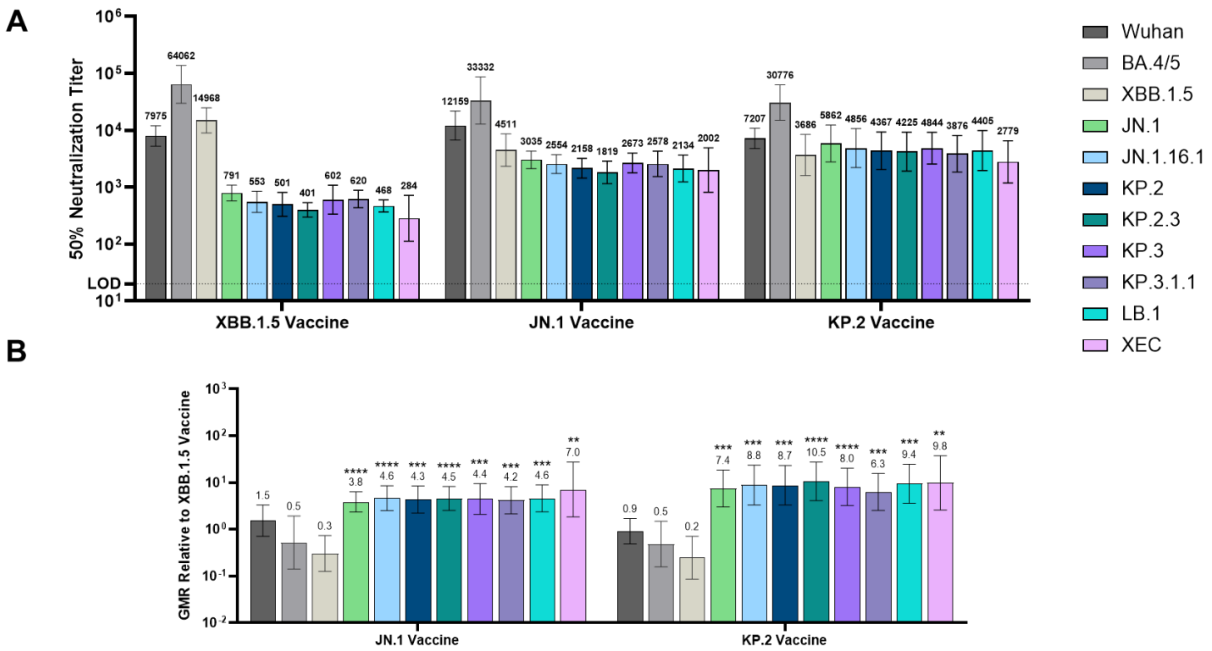

Figure 3. Pseudovirus Neutralization Elicited by BNT162b2 XBB.1.5, JN.1 And KP.2-Adapted Vaccines Administered to Vaccine-Experienced Mice. Female mice were immunized i.m. according to Fig. S4A on Days 0 and 21 with the BNT162b2 Wuhan (WT), on Day 49 with the bivalent BNT162b2 (WT + BA.4/5), on Day 84 with BNT162b2 XBB.1.5, and on Day 111 with the BNT162b2 XBB.1.5, JN.1, or KP.2 vaccine. One month post-5th dose, sera were collected from the terminal bleed and neutralizing antibody responses were measured against a panel of 11 pseudoviruses that included the Wuhan (WT) reference strain and Omicron lineages BA.4/5, XBB.1.5, JN.1, JN.16.1, KP.2, KP.2.3, KP.3, KP.3.1.1, LB.1, and XEC. **a** The number above each bar indicates the 50% neutralizing geometric mean titer (GMT) with 95% CI of 10 mice per vaccine group. **b** The geometric mean ratio (GMR) is shown as the ratio of the BNT162b2 KP.2 or JN.1 vaccine GMT to the BNT162b2 XBB.1.5 vaccine GMT of the corresponding pseudovirus. The number above each bar indicates the GMR with 95% CI. The limit of detection (LOD) is the lowest serum dilution, 1:20. Asterisks indicate statistical significance of pseudovirus GMR relative to the corresponding pseudovirus in the monovalent XBB.1.5 vaccine group. ****p<0.0001, ***p<0.001, ** p<0.01, * p<0.05.

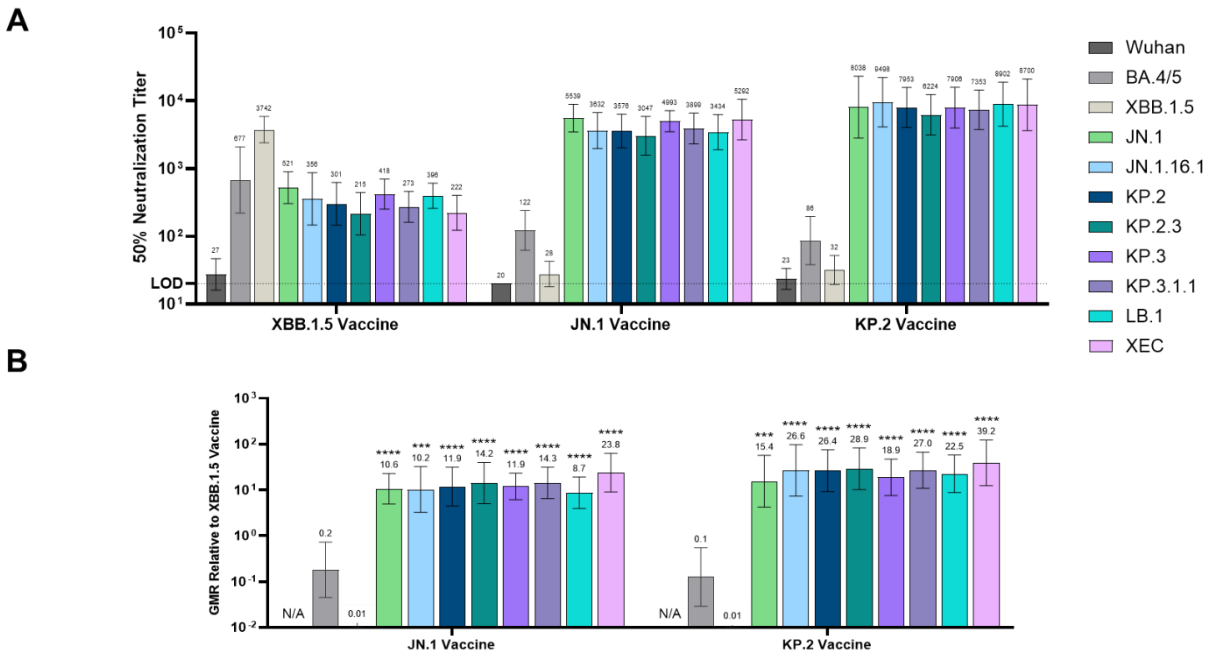

847

848 **Figure 4. Pseudovirus Neutralization Elicited by BNT162b2 XBB.1.5, JN.1 and KP.2-**
849 **Adapted Vaccines Administered as a Primary Series to Naïve Mice**. Female mice were
850 immunized i.m. according to Fig. S4A on Days 0 and 21 with the BNT162b2 XBB.1.5, JN.1, or
851 KP.2-adapted vaccine. Sera were collected from the terminal bleed (Day 49) and neutralizing
852 antibody responses were measured against a panel of 11 pseudoviruses that included the Wuhan
853 (WT) reference strain and Omicron lineages BA.4/5, XBB.1.5, JN.1, JN.16.1, KP.2, KP.2.3,
854 KP.3, KP.3.1.1, LB.1, and XEC. **a** The number above each bar indicates the 50% neutralizing
855 geometric mean titer (GMT) with 95% CI of 10 mice per vaccine group. **b** The geometric mean
856 ratio (GMR) is shown as the ratio of the BNT162b2 KP.2 or JN.1 vaccine GMT to the
857 BNT162b2 XBB.1.5 vaccine GMT of the analogous pseudovirus. The number above each bar
858 indicates the GMR with 95% CI. The limit of detection (LOD) is the lowest serum dilution,
859 1:20. Asterisks indicate statistical significance of pseudovirus GMR relative to the analogous
860 pseudovirus in the monovalent XBB.1.5 vaccine group. ****p<0.0001, ***p<0.001, ** p<0.01,
861 * p<0.05. N/A = Not available as both values to calculate GMR are at limit of detection.

862

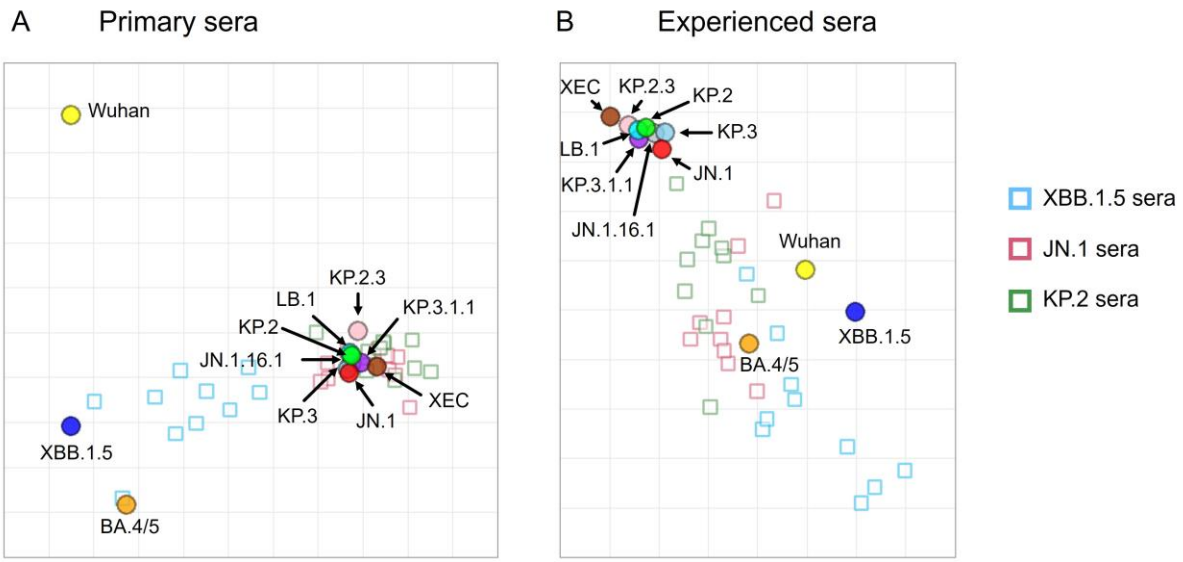

Figure 5. Antigenic Map of SARS-CoV-2 Omicron JN.1 Lineages Relative to Lineages Contained in Prior BNT162b2 Lineage-Adapted Vaccines. a-b Antigenic map visualizes cross-reactivity among a panel of 11 SARS-CoV-2 lineages showing **(a)** three groups of post-vaccination sera from naïve mice and **(b)** three groups of post-vaccination sera from vaccine-experienced mice. SARS-CoV-2 lineages are shown as circles and sera are indicated as squares. Each square corresponds to sera of one individual mouse and is colored by the vaccine that mouse received (BNT162b2 XBB.1.5, JN.1, or KP.2). Antigenic distance is represented in both horizontal and vertical axes. Each square in the matrix represents 1 antigenic unit, which reflects a two-fold difference in neutralization titer. The points that are more closely together reflect higher cross-neutralization and are therefore antigenically more similar.

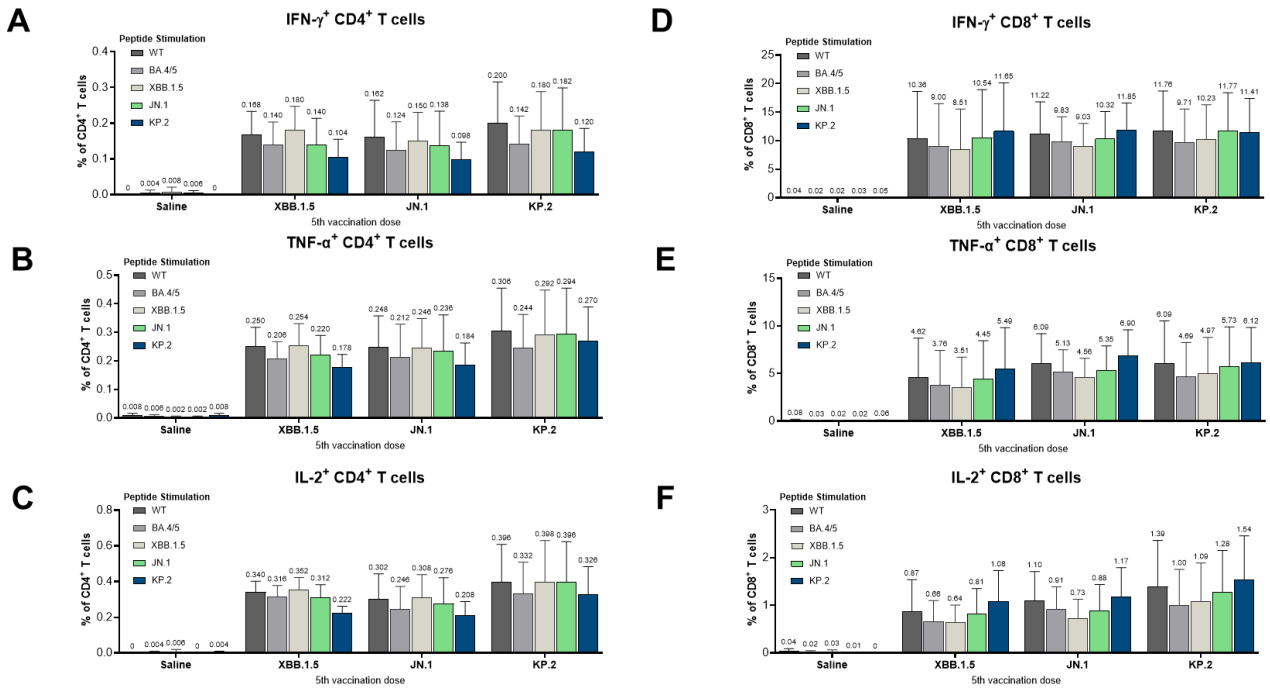

Figure 6. T Cell Mediated Immune Response Elicited by BNT162b2 XBB.1.5, JN.1 and KP.2-Adapted Vaccines Administered to Vaccine-Experienced Mice. One-month after the 5th dose of BNT162b2 variant-adapted vaccine (XBB.1.5, JN.1, or KP.2), S-specific splenocytes (n=5/group) were characterized by a flow cytometry-based intracellular cytokine staining (ICS) assay. All samples were stimulated *ex vivo* with S peptide pools from the WT reference strain and Omicron BA.4/5, XBB.1.5, JN.1, and KP.2 sublineages. **a-f** Graphs show the frequency of $CD4^+$ T cells expressing **(a)** IFN-γ , **(b)** TNF-α , and **(c)** IL-2 , and the frequency of $CD8^+$ T cells expressing **(d)** IFN-γ , **(e)** TNF-α , **(f)** IL-2 in response to stimulation with each peptide pool across vaccine groups. Bars depict mean frequency + SEM.

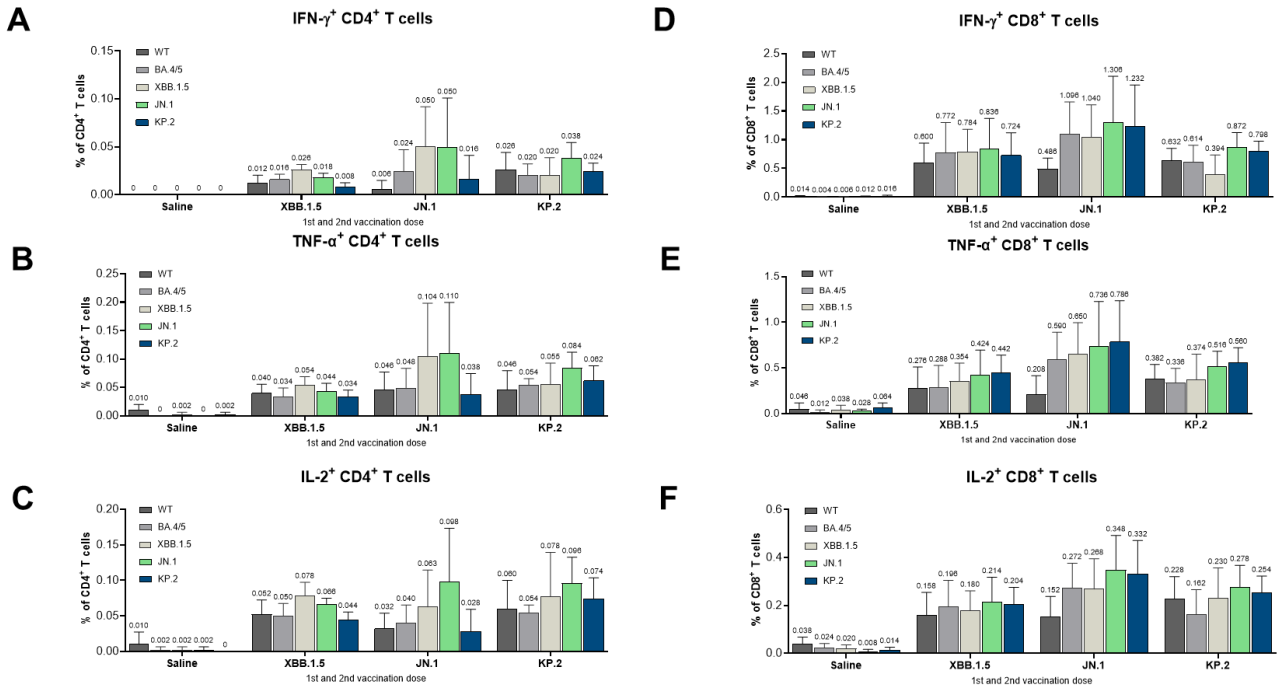

Figure 7. **T Cell Mediated Immune Response Elicited by BNT162b2 XBB.1.5, JN.1 and KP.2-Adapted Vaccines Administered to Naïve Mice**. At one-month post-second dose of BNT162b2 variant-adapted vaccine (XBB.1.5, JN.1, or KP.2) (completion of primary series), S-specific splenocytes (n=5/group) were measured by intracellular cytokine staining (ICS) assay. All samples were stimulated *ex vivo* with S peptide pools from the WT reference strain and Omicron BA.4/5, XBB.1.5, JN.1, and KP.2 sublineages. **a-f** Graphs show the frequency of $CD4^+$ T cells expressing **(a)** IFN-γ, **(b)** TNF-α ,and **(c)** IL-2 , and the frequency of $CD8^+$ T cells expressing **(d)** IFN-γ, **(e)** TNF-α , **(f)** IL-2 in response to stimulation with each peptide pool across vaccine groups. Bars depict mean frequency + SEM.

897 **Table 1. Emerging N-link glycosylation sites at JN.1 and KP.2 Spike proteins**

Variant	Mutation	Peptide	% Glycosylation
JN.1	K356T	R.FASVYAW**N**R.**T**	99.8%
	H245N	R.FQTLLAL**N**R.**S**	99.6%
KP.2	K356T	W.**N**R**T**RISNCVADY.S	98.3%
	H245N	R.FQTLLAL**N**R.**S**	96.2%

898